Modeling

Data Assimilation

Impact of QuikSCAT Data on Numerical Weather Prediction

One of the important applications of satellite surface wind observations is to increase the accuracy of weather analyses and forecasts. Satellite surface wind data can improve numerical weather prediction (NWP) model forecasts in two ways. First, these data contribute to improved analyses of the surface wind field, and, through the data assimilation process, of the atmospheric mass and motion fields in the free atmosphere above the surface. Second, comparisons between the satellite-observed surface wind data and short-term (6-hr) forecasts can provide information to improve model formulations of the planetary boundary layer, as well as other aspects of model physics.

The SeaWinds scatterometer on the QuikSCAT satellite was launched in July 1999, and it represents a dramatic departure in design from the other scatterometer instruments launched during the past decade (ERS-1 and 2 and NSCAT). The NASA DAO was the first data assimilation center to assimilate QuikSCAT SeaWinds data and evaluate their impact on numerical weather prediction. Following the launch of QuikSCAT, a detailed evaluation of the initial surface wind data sets was performed as part of a collaborative project between the Environmental Modeling Center of NCEP, NESDIS and the DAO. The first component of this evaluation consisted of both subjective and objective comparisons of QuikSCAT winds to ship and buoy observations, GEOS and NCEP wind analyses, ERS-2 wind vectors, and SSM/I wind speeds. This was then followed by a series of data assimilation and forecast experiments using the GEOS and operational NCEP data assimilation systems (DAS). The experiments were aimed at comparing the impact of QuikSCAT with that previously obtained with NSCAT (NASA Scatterometer), and at assessing the relative utility of QuikSCAT, SSM/I, and ERS-2 winds, the relative contributions of QuikSCAT directional and speed information, and the effectiveness of the QuikSCAT ambiguity removal algorithms.

For each DAS used, a control assimilation was generated using all available data with the exception of satellite surface winds. Then assimilations were generated that added one of the following: SSM/I wind speeds, QuikSCAT wind speeds, ERS-2 unique wind vectors, QuikSCAT ambiguous wind vectors, QuikSCAT unique wind vectors, or the combination of QuikSCAT with ERS-2 and SSM/I. This initial evaluation of QuikSCAT demonstrated potential for QuikSCAT data to improve meteorological analyses and forecasts. However, the evaluation also indicated ambiguity removal and rain contamination problems that were limiting the application of QuikSCAT winds to data assimilation.

As an illustration of the impact of QuikSCAT data, Figure 6-51 shows anomaly correlations for a limited sample of Control and QuikSCAT 500 mb height forecasts. From this figure, it can be seen that there is a slight positive impact of QuikSCAT in the Northern Hemisphere and a larger positive impact in the Southern Hemisphere.

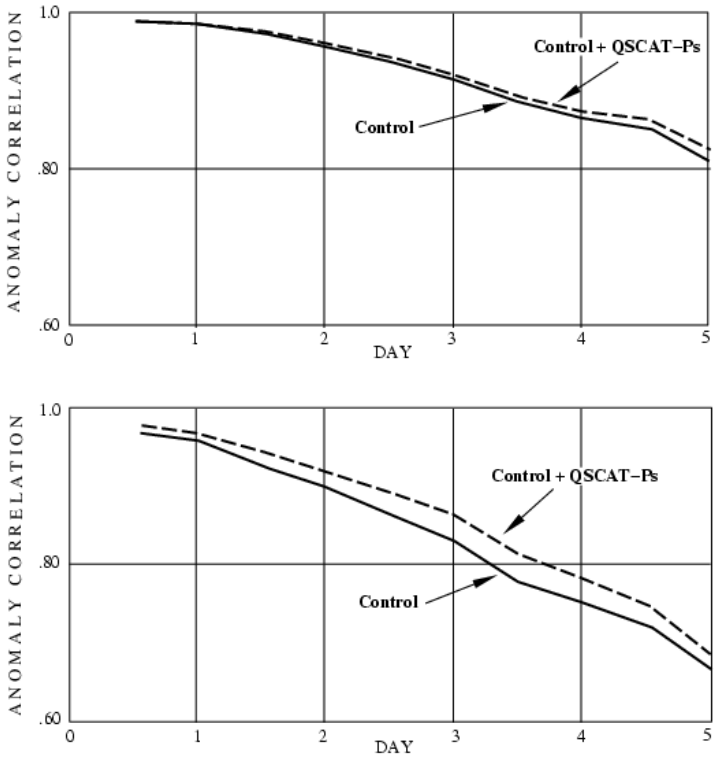

Figure 6-51. Anomaly correlations for a limited sample of Control and QuikSCAT 500 mb height forecasts. Upper panel Northern Hemisphere, lower panel Southern Hemisphere.

Robert Atlas Code 910.3 (Robert.M.Atlas.1@gsfc.nasa.gov)

Monitoring of Observation Errors Using the GEOS Ozone Assimilation System

We used the ozone assimilation system at the DAO to monitor error characteristics of ozone observations. This system assimilates the Total Ozone Mapping Spectrometer (TOMS) total column ozone and the Solar Backscatter UltraViolet/2 (SBUV/2) instrument ozone profiles into an off-line transport model. The system is providing near real-time global 3-dimensional ozone fields. In addition, the system routinely produces observed minus-forecast (O-F) residuals, i.e., the differences between observations and a short-term forecast. We used the O-F residuals to evaluate how well an observational data set agrees with the prediction model forecast and with other observational data. We found several examples of changes in observation error characteristics from time series of the O-F statistics.

One of the first examples was an abrupt change that occurred in the NOAA-14 SBUV/2 O-F residuals on March 31, 2000. Figure 6-52 shows the global mean of the O-F residuals for the ozone layer between 16 and 32 hPa. The sharp increase on March 31 was caused by a change in the SBUV/2 instrument calibration. After the SBUV/2 instrument team readjusted the calibration coefficients and reprocessed the data, we used the reprocessed SBUV/2 data in the assimilation. We found that the change in the global mean O-F value was significantly smaller with the reprocessed data. The change was almost within the typical variability of daily statistics. This finding indicates that reprocessed SBUV/2 data are more consistent with the SBUV/2 data before the calibration change. The calibration coefficients used in the reprocessing were later implemented by NOAA in the operational retrievals.

Another monitoring example shows the cross-track differences in Earth Probe TOMS data. TOMS is a scanning instrument that measures total column ozone. The observing geometry is unique for each scan angle, and some of the ozone errors are related to the scan angle at which a measurement is made. This scan-angle dependence increased in the beginning of 2001. The dependence is easiest to see in the tropics where natural zonal variability of the total column ozone is small. This scan-angle dependence is also evident in the O-F residuals from the assimilation system. A scatter plot of TOMS O-F residuals at 2 degrees south latitude reveals a larger cross-track bias in 2001 than in 2000 (Figure 6-53). This work demonstrates the use of the assimilation system to monitor TOMS data quality.

We have implemented monitoring of ozone observations from the Upper Atmosphere Research Satellite Microwave Limb Sounder. We plan to extend the monitoring and include ozone data from instruments on future satellites: EOS Aqua, EOS Aura, and European Space Agency Environment Satellite (Envisat).

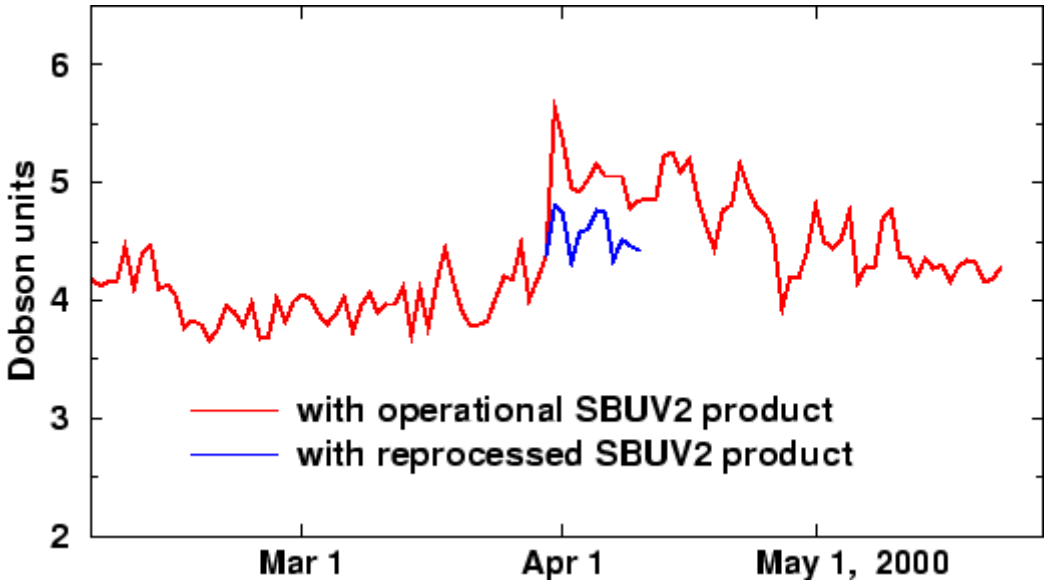

Figure 6-52. Time series of a daily global mean of O-F residuals for ozone column between 16 and 32 hPa from NOAA-14 SBUV/2 instrument is shown (red). The calibration changed on March 31. The mean of O-F residuals for SBUV/2 data reprocessed using a different calibration is shown in blue.

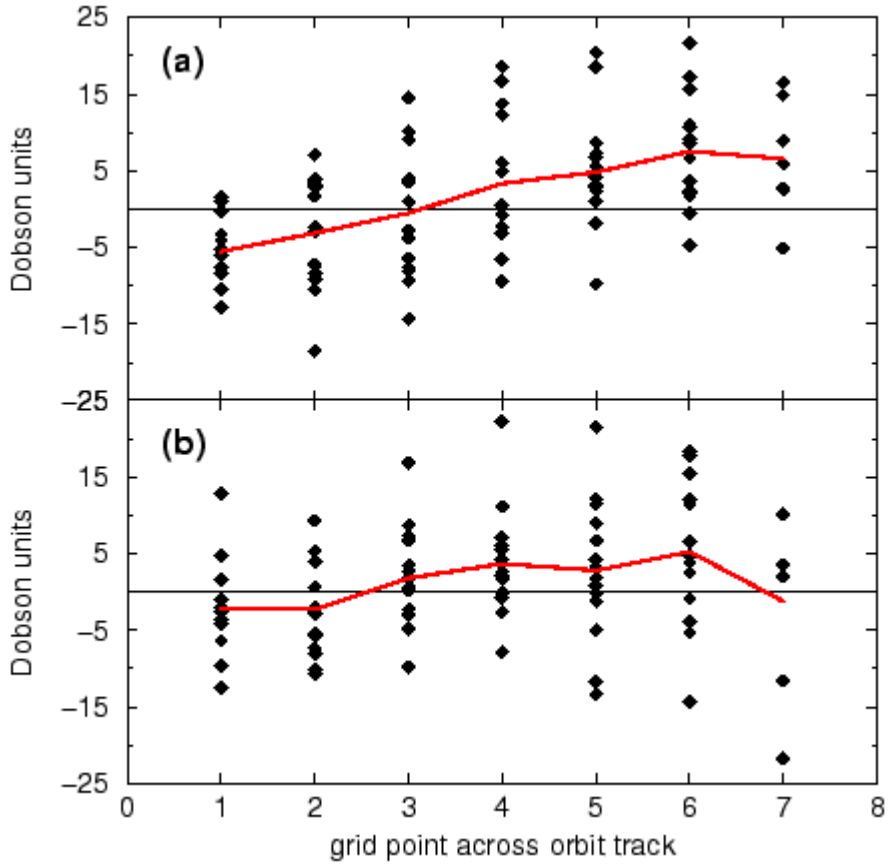

Figure 6-53. The TOMS O-F residuals at 2 degrees south latitude were binned by model grid points across the orbit track. The westernmost grid point is denoted by 1 and the easternmost one by 7. The residuals from 14 orbits on January 28 are shown by black diamonds for 2001 in a), and 2000 in b). The mean of residuals for each grid point is shown by the red curve. Across-track variability of the mean increased from 7.6 DU in 2000 to 13.1 DU in 2001.

Ivanka Stajner, 910.3 (Ivanka.Stajner.1@gsfc.nasa.gov)

Assimilation of Cloud- and Land-Affected Satellite Sounding Data at the Data Assimilation Office

Satellite data from passive microwave and infrared sounders consistently improve forecasts and analyses in data assimilation systems. However, most numerical weather prediction (NWP) centers use only a small fraction of the data available from these instruments. In particular, NWP centers often exclude data from infrared instruments, which are affected by clouds more than are microwave sensors. Similarly, most NWP centers omit data from land-affected channels.

Sensitive areas for medium-range forecasts are frequently cloudy. Clouds affect ~80% of infrared pixels from the Advanced TIROS Operational Vertical Sounder (ATOVS) flying on NOAA weather satellites. Conservative cloud detection schemes may declare 90% or more pixels as cloud-contaminated.

The next generation of infrared kilo-channel sounders offers more information than the current ATOVS infrared sounding instruments. This next generation includes the Atmospheric Infrared Sounder (AIRS), which will fly on the NASA EOS Aqua satellite. Our ability to use land- and cloud-affected data from these instruments may increase their impact on forecasting capabilities.

Several methods exist for utilizing cloud-affected data in a data assimilation system. These include (1) directly assimilating the cloudy radiances and (2) assimilating cloud-cleared radiances. Direct assimilation of cloudy radiances is very challenging, as it requires reasonably accurate model-generated clouds and a fast and accurate radiative transfer model. At the NASA DAO, we examined the latter approach.

Assimilating cloud-cleared radiances involves estimating the clear-column radiance that would have been observed in the absence of cloud. We examined the effectiveness of this approach using the DAO's next-generation finite-volume Data Assimilation (fvDAS) with a 1D variational radiance assimilation scheme. This system simultaneously performs cloud-clearing and retrieves information about temperature, humidity, ozone, and surface parameters including the surface skin temperature. The fvDAS experimental setup was at a resolution of 2° latitude × 2.5° longitude for the month of August 1999 with a 2-week spin-up. We conducted a series of experiments using different ATOVS data: (1) DAO CC (includes cloud-cleared data), (2) DAO CLR (clear data only), and (3) NESDIS (operational retrievals). One major caveat is that the DAO experiments used the NOAA 15 satellite with the Advanced Microwave Sounding Unit (AMSU) whereas the NESDIS experiment did not.

Figure 6-54 shows the spatial RMS of the bias and the standard deviation of the radiosonde observed minus 6-hour forecast residuals for heights. Figure 6-55 shows the standard deviations of the same for zonal and meridional winds. Both the DAO CC and DAO CLR have substantially less height bias. The DAO CC has a smaller bias in height in all regions except Asia (NE), where the type of radiosonde used has known temperature bias. The 6-hour forecast fit to radiosonde winds is best for the DAO CC case. Improvements in 5-day forecasts with DAO CC were also achieved.

Similar experiments were conducted with and without land-affected channels. A positive but smaller impact was shown on the 6-hour forecast heights and winds.

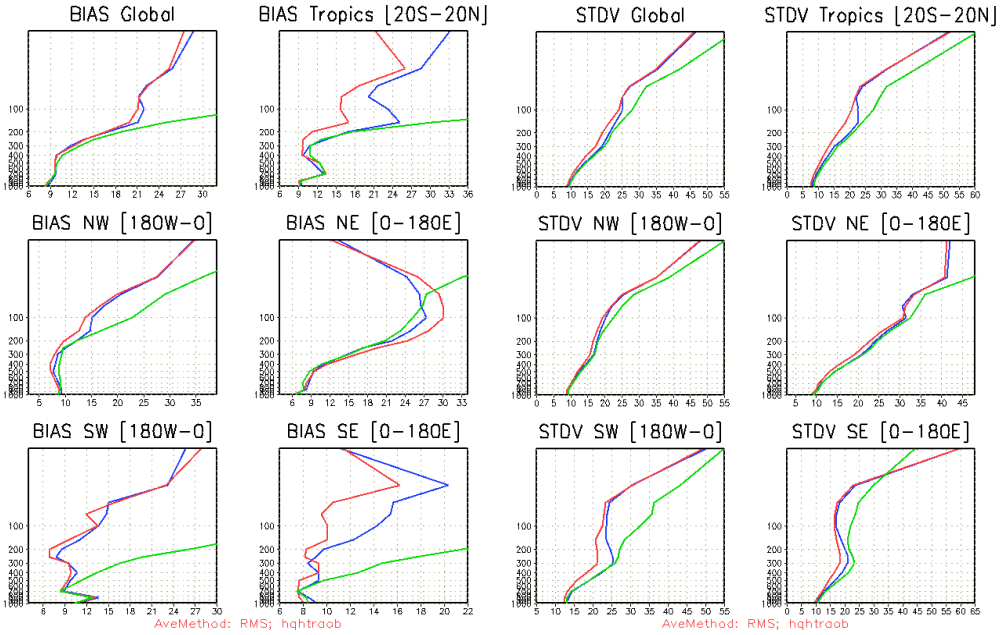

Figure 6-54. Spatial RMS of the bias (left) and standard deviation (right) of radiosonde observed heights minus 6 hour forecast residuals averaged over August 1999. Red: DAO CC; Blue: DAO CLR; Green: NESDIS.

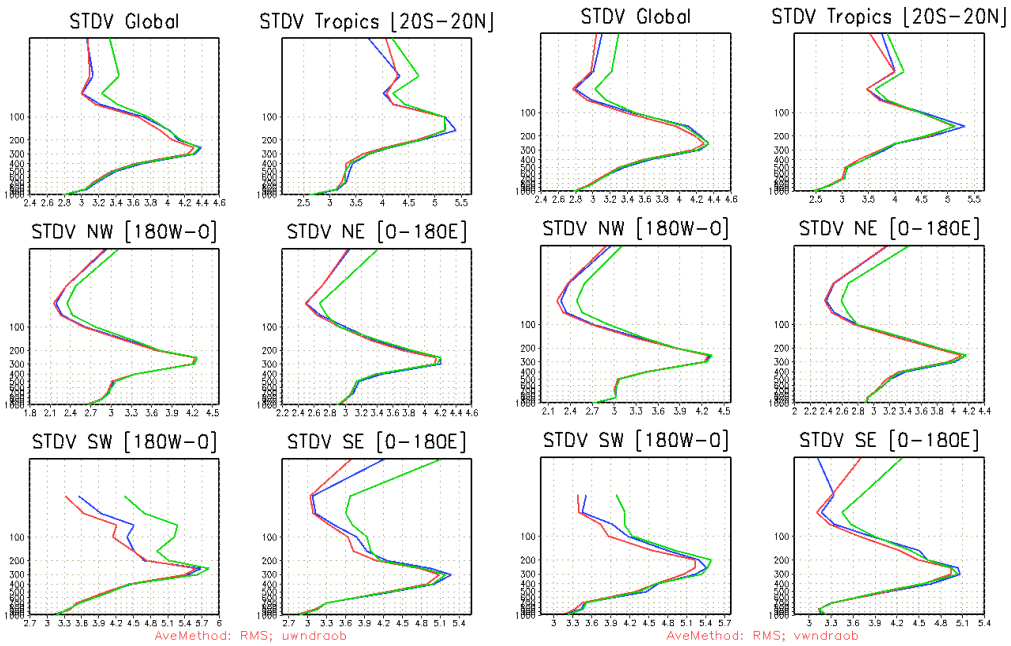

Figure 6-55. Standard deviation of radiosonde observed winds minus 6-hour forecast averaged over August 1999; Left: zonal (U) winds, Right: meridional (V) winds. Red: DAO CC; Blue: DAO CLR; Green: NESDIS

Joanna Joiner, Donald Frank, and Arlindo da Silva, Code 910.3 (Joanna.Joiner.1@gsfc.nasa.gov)

A Simple Framework for Assessing the Information Content of Observations from a Satellite Doppler Wind Lidar

It is by now well documented that perhaps the most important missing piece of observational information about the atmosphere is a global set of independent (i.e., nonmass-derived) vertical wind profiles in the free atmosphere, especially away from the regions of reasonably dense radiosonde coverage. Since the goal is to achieve a fairly high and uniform horizontal resolution, this can only realistically be achieved with a satellite system. A spaceborne Doppler Wind Lidar (DWL) is a candidate instrument, but numerous issues remain to be resolved before a final decision can be made.

In general, the design, development, deployment, and subsequent operation of a satellite instrument represent substantial investment. Therefore, decision makers are eager for tools that can help them assess the value and impact of a proposed new instrument as early as possible in its life cycle. This capability can provide input not only to the overall decision process on whether or not to proceed with a given instrument, but it can also support trade-off studies in the instrument-definition phase.

The established technique for doing such assessments in the field of Numerical Weather Prediction (NWP) is through Observing System Simulation Experiments (OSSEs). In OSSEs, observations are simulated from the proposed system and from the components of the already existing observing systems. These observations are then assimilated into a numerical model. Such experiments are expensive and time-consuming to set up and carry out. They therefore allow for only a limited amount of experimentation. Certain aspects of an instrument can be studied in simpler, less expensive frameworks that offer the possibility of a wider range of experiments while still maintaining some of the essential characteristics of the full testing environment.

In the DAO, we have developed such a framework specifically to measure the information content of a proposed Doppler Wind Lidar instrument in the context of a simplified meteorological analysis. The main target application of a DWL instrument is data assimilation. Thus, we have decided to judge the value of various simplified, idealized configurations of the instrument by their respective contributions to reducing the uncertainty of our knowledge of the state of the atmosphere; i.e., the *analysis error* in data assimilation terminology.

In this simplified testing framework, the user specifies a “true” wind field as well as a background wind field. The system then simulates and analyzes DWL observations at a given resolution and with given error characteristics. Since we know the true field, we can calculate the analysis error directly. Figure 6-56 shows an example of a simple true state (zonal flow with single eddy).

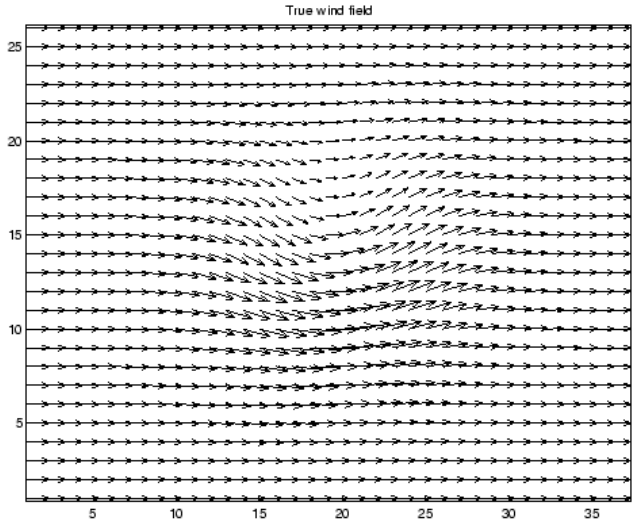

Figure 6-56. Example of a simple true state zonal flow with single eddy.

One of the most important issues studied with the system is the relative information content of single- vs. dual-perspective observations. A DWL only measures a single component of the flow; namely, the one that falls along a line of sight from the instrument down to the air parcel for which the flow is measured. It would thus take two independent measurements along different directions to uniquely determine the horizontal wind vector at a given point. This requirement would complicate the design of the instrument. We must, therefore, test whether—and in that case how—we might relax the requirement for two independent measurements per location.

Our experiments show clearly that single-perspective observations along parallel lines of sight are insufficient for retrieving the correct flow field with the given background field (compare the resulting analysis in Figure 6-57 with the true state from Figure 6-56). When both components of the wind are observed, the analysis quality improves dramatically (Figure 6-58). Interestingly enough, however, our results indicate that it is not necessary to obtain full knowledge of the wind vector at every single location, as long as the general flow field is observed along two separate directions. This finding demonstrates that the instrument must be able to observe along different directions, but not necessarily along more than one direction at any given location.

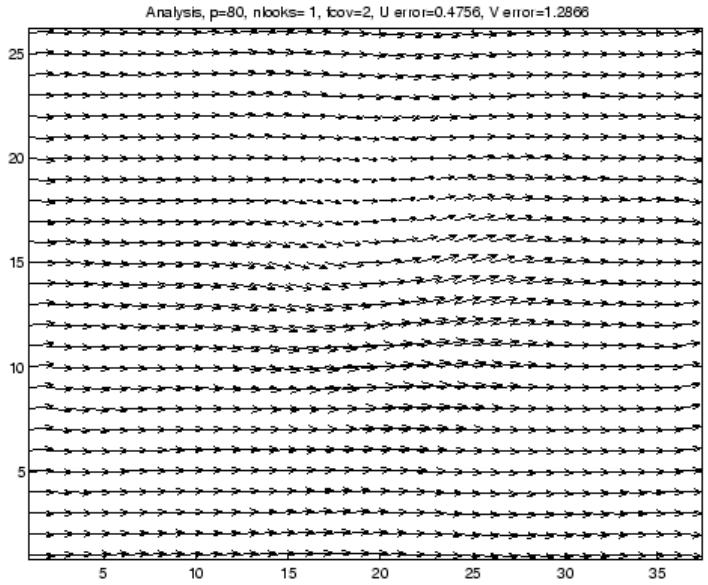

Figure 6-57. Flow field resulting from single-perspective observations along parallel lines of sight is shown to be insufficient for retrieving the correct flow field with the given background field (compare this with the true state from Figure 6-56).

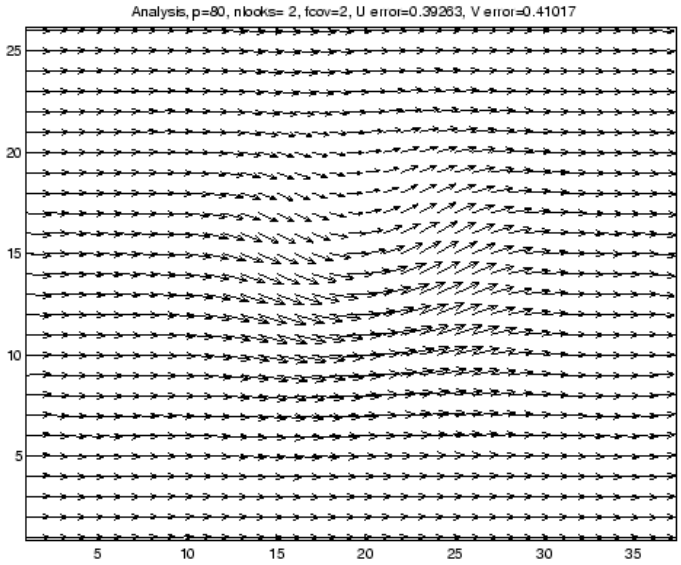

Figure 6-58. Flow field resulting from observation of both components of the wind, demonstrating a dramatic improvement of the analysis quality.

Satellite observation technology often involves a trade-off between the number and the accuracy of observations. Figure 6-59 illustrates how such a trade-off can be viewed from an analysis point of view. The isolines show the analysis error as a function of the number of observations (abscissa) and observation error (ordinate). Clearly, a given target analysis error can be obtained for a range of different combinations of measurement accuracy/number of measurements.

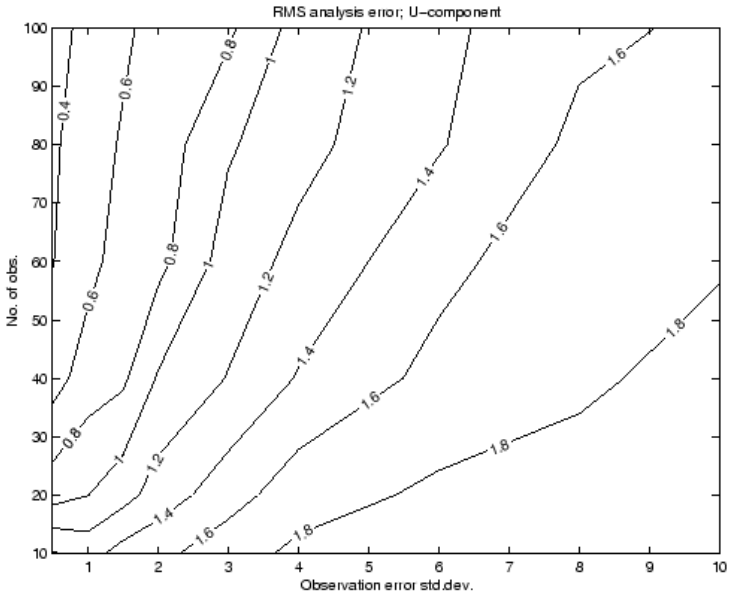

Figure 6-59. This figure illustrates how a trade-off between the number and the accuracy of observations can be viewed from an analysis point of view. The isolines show the analysis error as a function of the number of observations (abscissa) and observation error (ordinate).

Lars Peter Riishojgaard, Data Assimilation Office (Lars.P.Riishojgaard.1@gsfc.nasa.gov)

Water Vapor Tracers as Diagnostics of the Regional Hydrologic Cycle

NASA and other research institutions are deeply involved in assessing the effect of climate change on the water cycle. A key question remains: "Is the water cycle intensifying?" In other words, are climatic extreme events such as flood and drought increasing in frequency and intensity? Also, what are the local and remote sources of water for precipitation? This research addresses these questions by use of a diagnostic approach to quantitatively identifying the geographic source of water for precipitation in a general circulation model (GCM) and data analysis system (DAS).

We begin by implementing into the most recent Goddard Earth Observing System (GEOS) GCM a methodology for tracking regional water vapor (termed Water Vapor Tracers, WVTs). This methodology was originally developed at NASA GISS for global purposes (in mid-1980s). GEOS has state-of-the-art dynamical and physical processes and can be operated with much higher spatial resolution than the original GISS models (required to study precipitation and regions of the Earth). Regional WVTs provide quantitative information on the geographic sources of water for precipitation, including local and remote sources. The local source of water refers to water that is evaporated from a region, but precipitates before it leaves the region. This process is also known as "precipitation recycling" and is considered a potentially important feedback mechanism in the Earth's climate system.

Figure 6-60 shows several nearby geographical sources of water that supply Mexico and the North American monsoon system. As water enters the atmosphere from the surface of these regions, the WVT diagnostics maintain a mass balance that allows for the computation of precipitation from each region. For example, Figure 6-61 shows the simulated monthly mean annual cycle of precipitation area averaged for all of Mexico (from a 10-year GCM simulation). In addition, the figure shows the quantity of precipitation that occurs as a result of surface evaporation occurring from the nearby regions. The Mexico (MX) precipitation identifies the amount of precipitation recycling in this simulation. Recycling is considerable during most of the year, but largest during June, July, and August. The cross-equatorial transport of water from the South Pacific contributes to Mexican precipitation only during September and October.

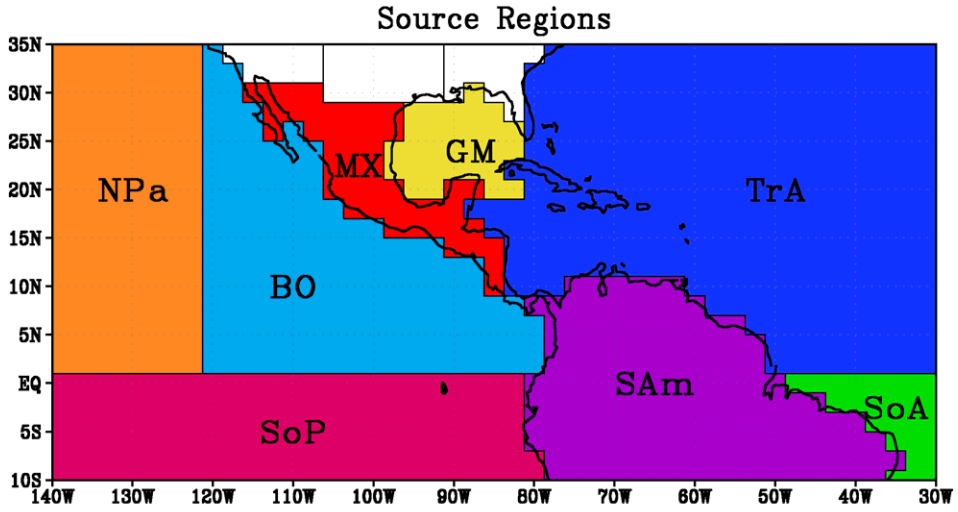

Figure 6-60. Geographic source regions of water that contributes to precipitation in Mexico. MX – Mexico, GM – Gulf of Mexico, TrA – Tropical Atlantic, SoA – South Atlantic, Sam – South America, SoP – South Pacific, BO – Baja Oceanic and NPa – North Pacific.

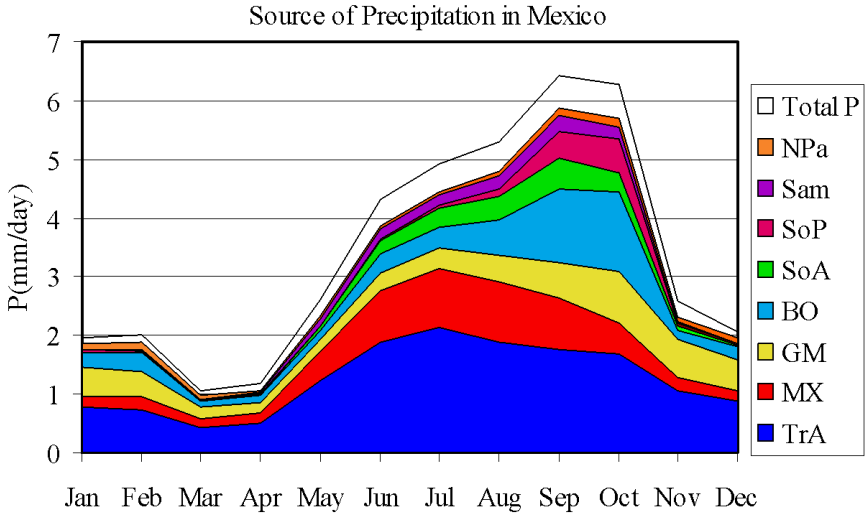

Figure 6-61. Amount of precipitation that fell in Mexico (MX) from nearby regions, as shown in Figure 6-60. All sources from the globe have been categorized, but only the eight largest sources are shown here. The largest sources are at the bottom and the smallest are at the top.

The full potential of this diagnostic method is only now being realized. The basic formulation has been validated and presented to the community (Bosilovich and Schubert, 2002). A project to better understand the hydrology of the North American Monsoon is ongoing. We are also attempting to use this methodology to identify the sources of water that contribute to the development and maintenance of hurricanes. We will use water vapor tracers to study the impact of remotely sensed water vapor on data assimilation.

Bosilovich, M.G. and S.D. Schubert, 2002: Water Vapor Tracers as Diagnostics of the Regional Hydrologic Cycle. *Journal of Hydrometeorlogy* (accepted, to appear in early 2002).

M.G. Bosilovich and S.D. Schubert, DAO, Code 910.3 (Michael.G.Bosilovich.1@gsfc.nasa.gov)

Retrospective Data Assimilation

The Laboratory for Atmospheres has developed a retrospective data assimilation system (RDAS) that we expect will produce data sets of a quality superior to that currently available for climate research. Retrospective data assimilation implements an advanced data assimilation technique that is an extension of the more common 3-dimensional variational procedure used operationally in the Laboratory and elsewhere.

Retrospective data assimilation is similar to four-dimensional variational assimilation. It uses the adjoint of the tangent linear of the dynamical atmospheric model to propagate observation and model information back in time. Thus, it allows users to refine estimates of the state of the atmosphere that are generated through standard procedures.

We illustrate in Figure 6-62 the potential benefits of retrospective data assimilation by comparing its results with those from our standard 3-dimensional variational assimilation system. We choose as a case study the meteorologically challenging French storm of 27 December 1999.

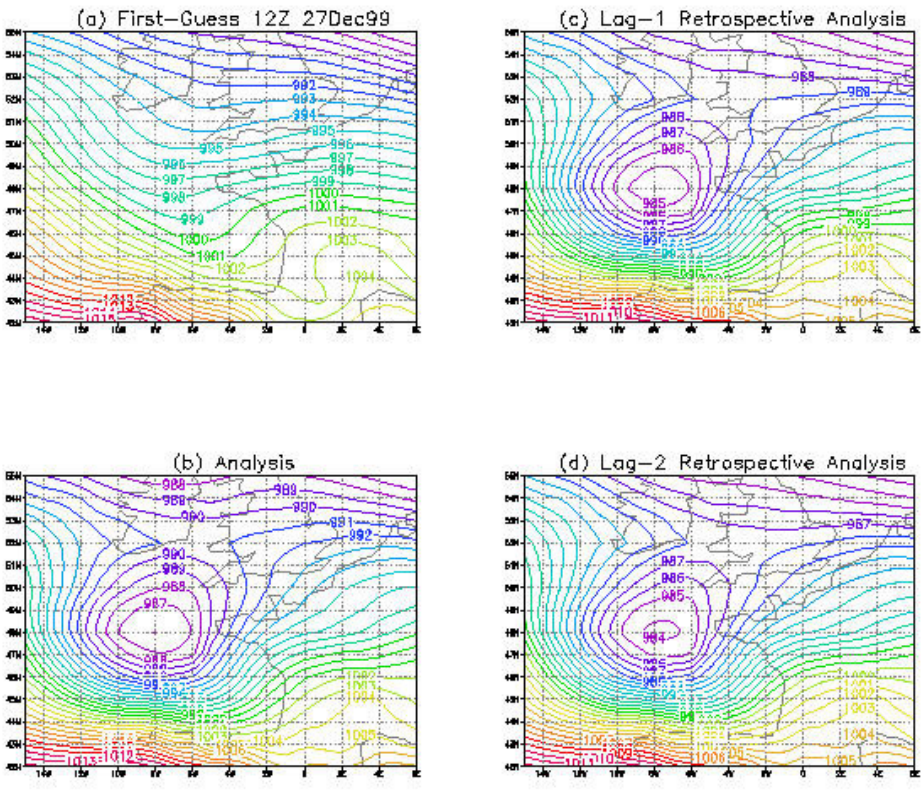

Figure 6-62 shows contours of sea level pressure, at 1 mb intervals, for 12 GMT 27 December 1999. The panels correspond to differently obtained estimates of the state of the atmosphere 6 hours before the peak of the storm. Panels (a) and (b) on the left are respectively the forecast and analysis generated by the standard assimilation system. The forecast is simply a 6-hour model prediction and does not contain any observational information. The analysis blends the 6-hour model prediction and the observations at 12 GMT. Because the analysis combines both model predictions and observations, it is generally a better estimate of what actually happens in the atmosphere than the forecast. Panels (c) and (d) on the right are the estimates of the state of the atmosphere obtained with the RDAS. These analyses are essentially a "redo" of the normal analysis [in panel (b)], and still valid at 12 GMT, but now are obtained using observational data taken after 12 GMT. For this reason, we call them retrospective analyses.

In ideal circumstances, when all assumptions in the theory are met, we expect retrospective analyses to be more accurate than the regular analysis, since they use an extended data set with observational data taken after the time of the event. Here, in the French storm illustration, we produce the lag-1 retrospective analysis of panel (c) using observations taken from 12 GMT to the time of the storm's peak at 18 GMT. We produce the lag-2 retrospective analysis of panel (d) using observations from 12 GMT to 00 GMT of the following day. An after-the-fact evaluation indicates that the regular analysis [panel (b)] overestimates the minimum of the low-pressure system by almost 9 mb. Therefore, the lag-2 RDAS analysis shows an improved low-pressure system. This improvement arises from the use of data taken after the time of the event and from the use of the adjoint of the tangent linear model of the atmospheric model that propagates this extra observational information back in time.

One of the goals of the Laboratory for Atmospheres is to generate an accurate, global, and continuous record of the state of the atmosphere. This record must be of very high quality. We consider retrospective data assimilation one possible technique to help us accomplish this goal.

Cohn, S.E., N.S. Sivakumaran, and R. Todling, 1994: A fixed-lag Kalman smoother for retrospective data assimilation. *Mon. Wea. Rev*., 122, 2838-2867.

Todling, R., S.E. Cohn, and N.S. Sivakumaran, 1998: Suboptimal schemes for retrospective data assimilation based on the fixed-lag Kalman smoother. *Mon. Wea. Rev.*, 126, 2274-2286.

Ricardo Todling, Code 910.3/SAIC (Ricardo.Todling.1@gsfc.nasa.gov)

Can We Predict the Next Dust Bowl?

Multiyear droughts are a regular feature of the Great Plains climate, having occurred once or twice a century over the last 400 years (Woodhouse and Overpeck, 1998). Laboratory scientists have recently gained insight into the nature and predictability of these events.

Our results are based on an ensemble of nine 70-year (1930–1999) simulations. We ran these simulations using the NASA Seasonal-to-Interannual Prediction Project (NSIPP-1) atmospheric-land general circulation model (AGCM). The simulations were run at a horizontal resolution of 2° latitude by 2.5° longitude and were forced by observed sea surface temperatures (SSTs). We also present results from some runs with idealized SST forcing. The model is part of the NSIPP coupled atmosphere-land-ocean model. However, for these experiments, we ran the model uncoupled from the ocean. Our focus is on assessing whether the model produces droughts in the Great Plains similar to those observed and, if so, to assess the nature and predictability of the simulated droughts.

The nine 70-year runs were forced with identical SSTs (the observed) and differ only in their initial atmospheric conditions: the initial conditions were chosen arbitrarily from previously completed simulations. Since all runs "see" the same SST forcing, the degree to which they produce similar results is an indication of predictability (assuming we have perfect knowledge of the SST). For example, if all runs produce identical precipitation variations in the Great Plains, we would conclude that precipitation in that region is perfectly predictable if we could somehow perfectly predict the SST.

Figure 6-63 shows the simulated precipitation over the Great Plains from all nine runs. The results are filtered to isolate time scales longer than about 6 years. Clearly, the nine ensembles produced varied results. The variation suggests that SST does not have a strong control on the precipitation in that region. Nevertheless, the runs do show some similarities. For example, during the 1930s almost all the runs show a tendency for dry conditions, consistent with the observations. This is followed, in the early 1940s, by wet conditions, again consistent with the observations. On the other hand, during the 1950s, the runs show a mixture of dry and wet conditions. Only one of the nine runs is as dry as observed. In general, the model results do agree with the observations in that the observations tend to fall within the spread of the ensemble members.

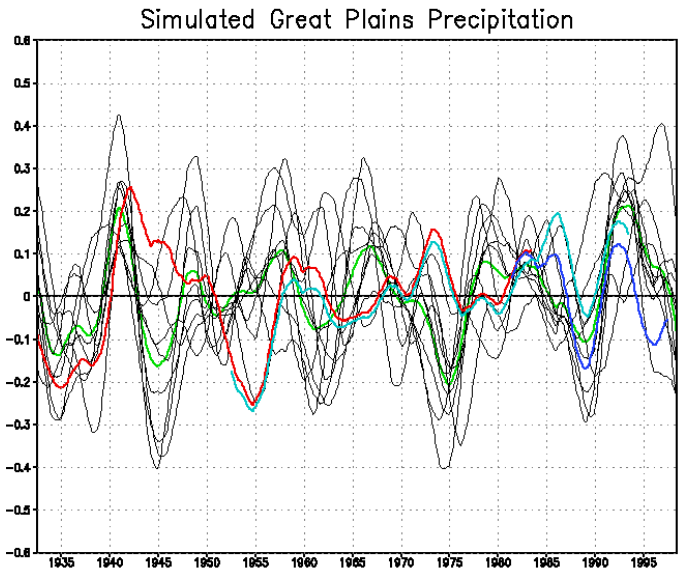

Figure 6-63. Time series of precipitation anomalies over the Great Plains (30°-50°N, 95°-105°W). A filter is applied to remove time scales shorter than about 6 years. The black curves are the results from the nine ensemble members produced with the NSIPP-1 model forced by observed SST. The green curve is the ensemble mean. All the other colored curves are various observational estimates.

We can obtain some idea of the connection between the Great Plains precipitation and the SST by correlating the ensemble-mean-filtered Great Plains precipitation (green curve in Figure 6-63) with the similarly filtered SST at all points. The correlations, with a sign change to emphasize the connection with dry conditions over the Great Plains (lower panel of Figure 6-64), show a large-scale coherent structure that has some similarity to the cold phase of an El Niño/Southern Oscillation (ENSO) event. Reduced precipitation in the Great Plains on these long time scales is associated with negative SST anomalies throughout the central tropical Pacific Ocean, extending northward toward the west coast of North America. The negative SST anomalies are flanked by positive anomalies that extend poleward and eastward from the western tropical Pacific.

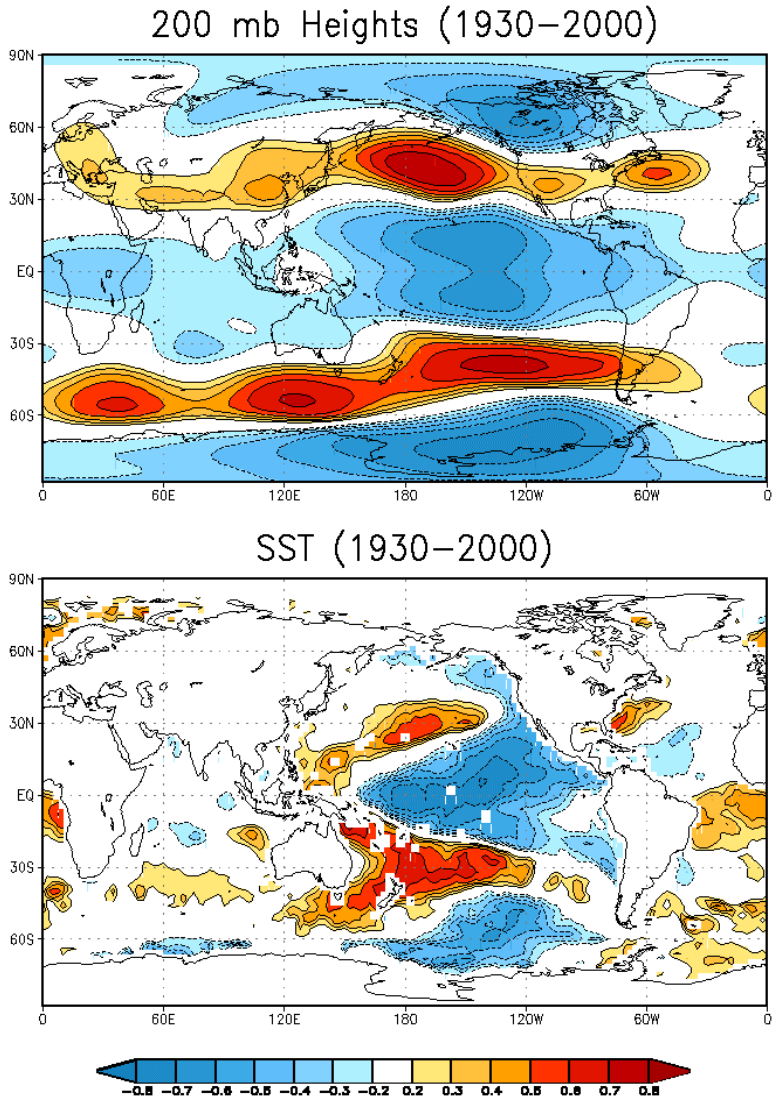

Figure 6-64. The negative of the correlation between the low-pass filtered ensemble mean simulated precipitation anomalies over the Great Plains (green curve in Figure 6-63) and 200mb height (top panel), and SST (bottom panel) for the period 1930–1999.

Figure 6-64 top panel shows the correlation between the filtered ensemble mean Great Plains precipitation and the filtered ensemble mean 200mb height field at all points. This shows that Great Plains precipitation is associated with global-scale height anomalies. Dry conditions are associated with positive height anomalies in the middle latitudes of both hemispheres, and reduced heights in the tropics and the high latitudes. We note that the zonally symmetric structure of the height anomalies found here is similar to that found on interannual time scales during northern summer (Schubert et al., 2001).

The above results suggest that low-frequency variations in Great Plains precipitation are, at least in part, controlled by large-scale pan-Pacific SST anomalies that resemble the correlation pattern shown in Figure 6-64 bottom panel. It turns out that the pan-Pacific SST pattern shown here is the dominant pattern of SST variability on these very long time scales (based on an empirical orthogonal function analysis–not shown). To further support this Great Plains/SST link, we have carried out several additional AGCM simulations in which the model is forced for 40 years by the positive and negative versions of the pan-Pacific SST anomalies shown in Figure 6-64 bottom panel. (We actually use +/- 2 standard deviations of the dominant SST empirical orthogonal function.) A third 40-year run was done with seasonally varying climatological SSTs (no anomalies). The results, shown in Figure 6-65, confirm that the cold phase of the pan-Pacific SST pattern tends to produce drier than normal conditions in the Great Plains, while the warm phase tends to produce wetter than normal conditions. Here, normal is defined as the average of the case with no SST anomalies (the straight black line in Figure 6-65).

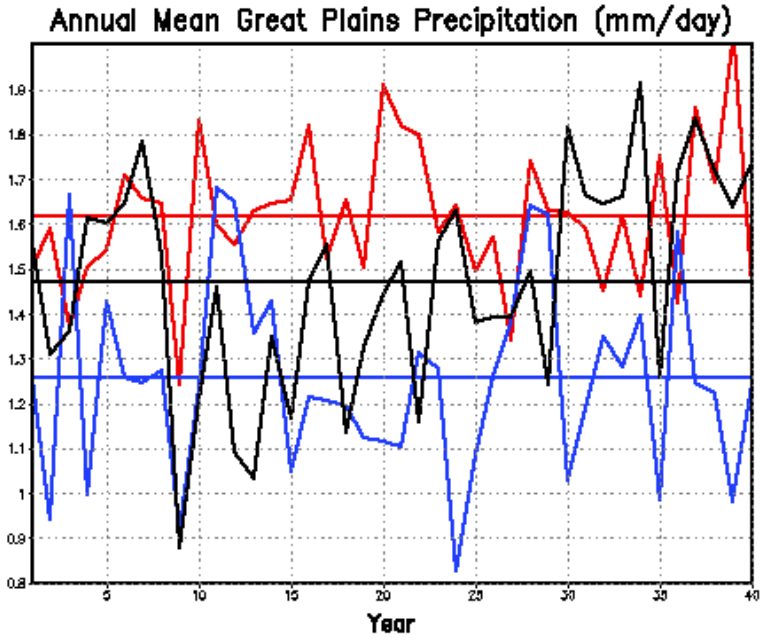

Figure 6-65. Model simulations of the annual mean precipitation over the United States Great Plains region (30°-50°N, 95°-105°W). In these idealized runs the model is forced by the global SST anomalies resembling those shown in Figure 6-64 (+/- 2 standard deviations). The red curve shows the results for the run forced by SST with positive anomalies in the tropical central Pacific (the warm phase). The blue curve shows the results for the run forced by SST with negative anomalies in the tropical central Pacific (the cold phase). The black curve is for the case with no anomalies. The straight lines are the corresponding 40-year means.

One rather remarkable and unexpected result from these idealized SST runs is that the case without SST anomalies (the black curve) exhibits rather pronounced multiyear precipitation variations. For example, during years 10–20 the Great Plains are nearly as dry as for the cold SST run, while during years 30–40 the Great Plains are wetter than that for the warm SST run. This suggests that the model is capable of producing multiyear (even decade-long) droughts in the absence of any nonseasonal SST variations.

This study shows that the NSIPP-1 model, when forced by observed SSTs, does produce low-frequency (multiyear) variations in the Great Plains precipitation similar to those observed. In particular, the model produces the dry conditions of the 1930s "dust-bowl" era. On the other hand, the model does not show a strong tendency for the dry conditions that were observed during the early 1950s (only one of the nine ensemble members reproduced the dry conditions). A correlative analysis suggests that the low-frequency variations in the Great Plains precipitation are linked to variations in a pan-Pacific decadal SST pattern. This was confirmed by further AGCM simulations, in which the model was forced by the 2 polarities of the Pacific SST pattern. These runs, as well as the nine 1930–1999 runs, show that when the Pacific decadal SST pattern is in its warm phase, the Great Plains tends to have above normal precipitation, while there is a tendency for drought during the cold phase.

The results suggest that our ability to predict the next dust bowl in the Great Plains will require predicting the long-term behavior of the pan-Pacific SST pattern. This is, however, only part of the story since the SSTs do not provide a strong constraint on the precipitation: this is clear from the spread in the curves shown in Figure 6-63. In other words, even if we could predict the SST perfectly, our precipitation forecast would still bear uncertainty that results from processes unrelated to the SST. In fact, our results suggest that precipitation in the Great Plains can exhibit very low-frequency (decadal time scale) variations even in the absence of SST anomalies. The nature of these variations and the implications for the predictability of drought in the Great Plains are currently under investigation.

Bark, D.L., 1978: History of American Droughts. *North American Droughts*. AAAA Selected Symposia Series. Westview Press, Boulder Colorado, N.J. Rosenberg, Ed., pp 9-23.

Borchert, J.R., 1971: The dust bowl in the 1970's. Assoc.Amer.Geogr.Ann., 61, 1-22.

Felch, R.E., 1978: Drought: Characteristics and assessment. *North American Droughts*. AAAA Selected Symposia Series. Westview Press, Boulder Colorado, N.J. Rosenberg, Ed., pp 25-42.

Felch, R.E., 1978: Drought: Characteristics and assessment. *North American Droughts*. AAAA Selected Symposia Series. Westview Press, Boulder Colorado, N.J. Rosenberg, Ed., pp 25-42.

Hughes, P., 1976: Drought: The land killer. American Weather Stories, U.S. Dept. Commerce, NOAA-EDS, Washington, D.C., pp 77-87.

Schubert, S.D., M.J. Suarez, P.J. Pegion, M.A. Kistler, and A. Kumar, 2001: Predictability of zonal means during boreal summer. To appear in *J. Climate*.

Woodhouse, C.A. and J.T. Overpeck 1998: 2000 years of drought variability in the central United States. *Bull.Amer.Meteor.Soc*., 79, 2693-2714.

Worster, D., 1979: Dust Bowl: The Southern Great Plains in the 1930s. Oxford University Press, New York, 277 pp.

Siegfried D. Schubert, Max J. Suarez, and Philip J. Pegion, Code 910.3 (Siegfried.D.Schubert.1@gsfc.nasa.gov)

High-Efficiency High-Resolution Global Model Development at the Data Assimilation Office

The DAO is leading the effort in the development of a new generation of ultrahigh-resolution GCMs that is suitable for 4-D data assimilation, numerical weather predictions, and climate simulations. These three areas of the model's application have conflicting requirements. For 4-D data assimilation and weather predictions, it is highly desirable to run the model at the highest possible spatial resolution (e.g., 55 km or finer) so as to be able to resolve and predict socially and economically important weather phenomena such as tropical cyclones, hurricanes, and severe winter storms. For climate change applications, the model simulations need to be carried out for decades, if not centuries. To reduce uncertainty in climate change assessments, the next generation model would also need to be run at a fine enough spatial resolution that can at least marginally simulate the effects of intense tropical cyclones. Scientific problems (e.g., parameterization of subgrid scale clouds) aside, all three areas of application require the model's computational performance to be dramatically enhanced as compared to the previous model generation.

Using a hybrid distributed-shared memory programming paradigm that is portable to virtually any of today's high-end parallel super computers, scientists at DAO have achieved unprecedented computing performance on the NCCS's SGI Origin-3000 machine. Figure 6-66 demonstrates the computational throughput (in model simulation days per wall clock day) of DAO's 55-level finite-volume GCM (fvGCM) at the 55 km horizontal resolution. Using this next generation high-resolution model for numerical weather predictions, a 10-day forecast can be done in 1 hour on the SGI Origin-3000 machine. Scientists at DAO are currently exploring ways to further increase the model's spatial resolution to 28 km while at the same time keeping the throughput at a rate that is still operationally feasible.

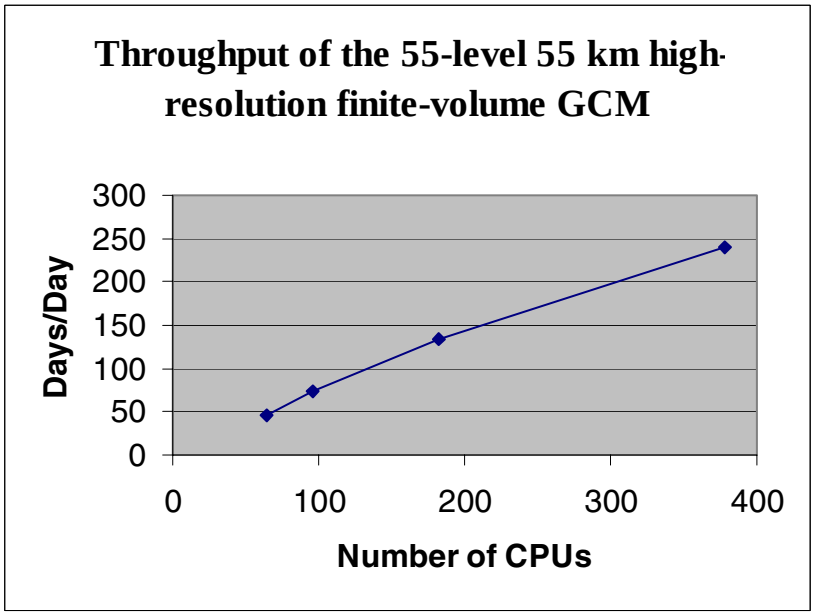

Figure 6-66 shows the computational throughput (in model simulation days per wall clock day) of DAO's 55-level finite-volume GCM (fvGCM) at the 55 km horizontal resolution.

Shian-Jiann Lin, Code 910.3 (Shian-Jiann.Lin.1@gsfc.nasa.gov)

Improving Global Analysis and Forecasts Using TRMM and SSM/I Observations of Precipitation Processes

Scientists at the Laboratory for Atmospheres have developed innovative techniques to assimilate, into global models, rain rates and total precipitable water (TPW) derived from space-based passive microwave sensors. Our results show that we can significantly improve the quality of GEOS analyses and short-range forecasts through variational assimilation of surface rain rates and TPW from TRMM Microwave Imager (TMI) and SSM/I using, as a control variable, the moisture tendency produced by the model physics.

Figure 6-67 shows the impact of assimilating 6-hour averaged TMI and SSM/I rainfall and TPW on GEOS analysis at 1° x 1° horizontal resolution for January 1998. The improved precipitation in the tropics effectively reduces the monthly-mean bias and standard deviation errors in the outgoing longwave radiation (OLR). OLR was not assimilated but was used for independent verification. Current global analyses contain significant errors in hydrological parameters. Thus, we see important implications in the result that rainfall assimilation improves not only precipitation but also related fields such as cloud and radiation. This work identifies precipitation as a key observation for improving the quality and usefulness of global analyses for understanding the Earth's water and energy cycles.

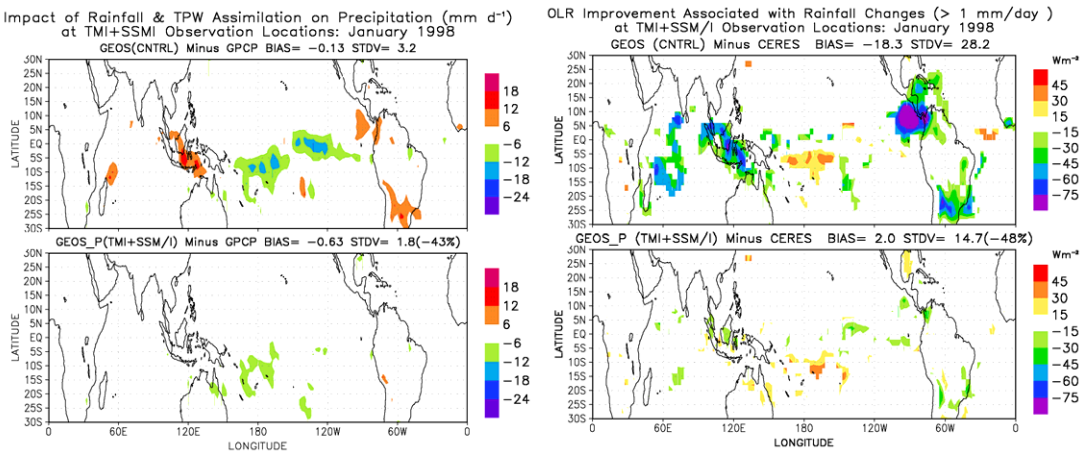

Figure 6-67. GEOS assimilation results with and without TMI and SSM/I observations for January 1998. Left panels show errors in the monthly-mean tropical precipitation fields verified against GPCP combined satellite-gauge estimate. Top is the difference between the GEOS control (without rainfall and TPW data) and GPCP. Bottom is the corresponding error in GEOS assimilation with rainfall and TPW data. Right panels show the impact on the outgoing longwave radiation (OLR) verified against CERES/TRMM measurements. Percentage changes in the tropical-mean error standard deviation relative to the GEOS control are given in parentheses.

The improved analysis with rainfall data also provides better initial conditions for storm-track and quantitative precipitation forecasts (QPF), as shown in Figure 6-68 for Hurricane Bonnie. Results from 5-day ensemble forecasts show systematic improvements in precipitation, divergent winds, and geopotential heights in the tropics. These results suggest that rainfall assimilation has the potential to significantly improve weather forecasting skills.

Laboratory scientists are currently developing techniques to assimilate the latent heating information together with precipitation data derived from microwave instruments into global models. This work will further improve short-range forecasts and assimilated global data sets for climate analysis.

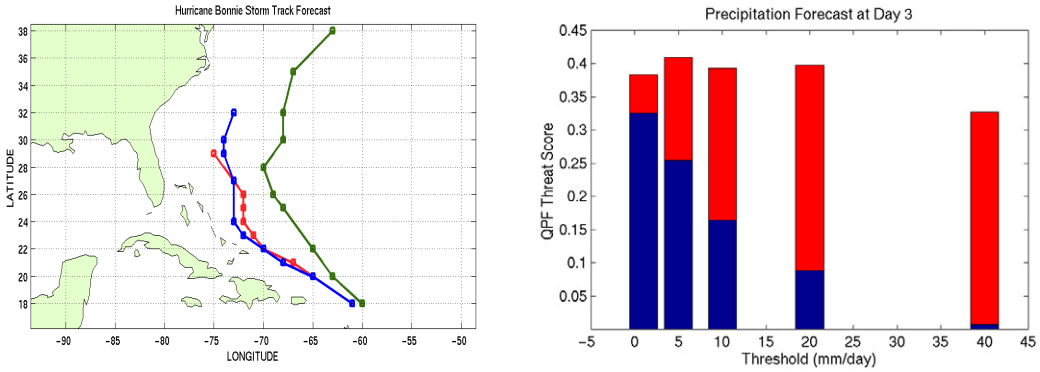

Figure 6-68. Improved storm track forecasts and QPF Equitable Threat Scores for Hurricane Bonnie. The left panel shows that the 5-day storm track forecast initialized with 1° x 1° GEOS analysis containing TMI and SSM/I rainfall data (blue) is in close agreement with the best track analysis from NOAA. The track from the control experiment is shown in green. The forecasts are initialized at 12:00 on 20 August 1998. The right panel shows the consistently higher Equitable Threat Scores for Day 3 precipitation forecast (red) initialized by the analysis with rainfall data. Results for the control experiment are shown in blue. A higher Threat Score corresponds to greater forecast skills.

Hou, A.Y., S. Zhang, A. da Silva, W. Olson, C. Kummerow, J. Simpson, 2001: Improving global analysis and short-range forecast using rainfall and moisture observations derived from TRMM and SSM/I passive microwave instruments. *Bulletin of Amer. Meteor. Soc.*, 82, 659-679.

Arthur Y. Hou, Code 910.3 (Arthur.Y.Hou.1@gsfc.nasa.gov)

Hurricanes

Simulation of the Cloud-Scale Structure of an Atlantic Hurricane

Hurricanes are well known for their high winds, heavy rainfall, and damaging storm surges. Along with the tolls they take in human lives and in property damage, they can also severely disrupt local economies, lead to housing and food shortages, cause problems with disease in flooded areas, and require massive disaster relief. Our ability to observe and forecast hurricanes has improved tremendously in recent decades as a result of satellite measurements and improved numerical models. We can now observe the occurrence of hurricanes all over the planet and can provide reasonably good forecasts of hurricane tracks. Yet we are still far from being able to accurately forecast rapid changes in storm intensity, partly because of insufficient observations of the processes that contribute to intensification as well as a lack of knowledge about how such intensification occurs.

We have simulated a hurricane using a numerical weather prediction model for the purpose of examining the processes that contribute to storm structure and intensification. Unlike many previous simulations of hurricanes in which clouds were either completely parameterized or only coarsely resolved, this simulation uses a horizontal grid spacing that is capable of resolving individual clouds.

The model produces a realistic hurricane (Figure 6-69) that intensifies slowly during the period of simulation and provides insight into factors influencing storm structure. The hurricane wind field is composed of a primary circulation that is associated with the strong, damaging winds that move tangentially around the storm center. A secondary circulation includes a circuit with radial inflow near the surface, rising motion in the wall of thunderstorms that surrounds the eye (known as the eyewall), and outflow in the upper troposphere. We find that the general structure of the storm is determined partly by characteristics of the storm's environment and also by dynamical instabilities induced by the hurricane's primary circulation. Vertical and horizontal variations in the environmental winds influence the structure of the storm by favoring near-surface inflow, rising motion in the eyewall, and precipitation on the west-northwestern side of the storm. While the storm's environment favors one side of the storm, a dynamical instability develops in the eyewall associated with radial changes in the primary circulation. This instability produces a pair of lower- and higher-pressure regions in the eyewall (Figure 6-69) that rotate around the center at about half the speed of the vortex winds. Counter-clockwise and clockwise wind perturbations occur with these low- and high-pressure anomalies, respectively, and influence the patterns of inflow and outflow, upward motion, and precipitation in the eyewall.

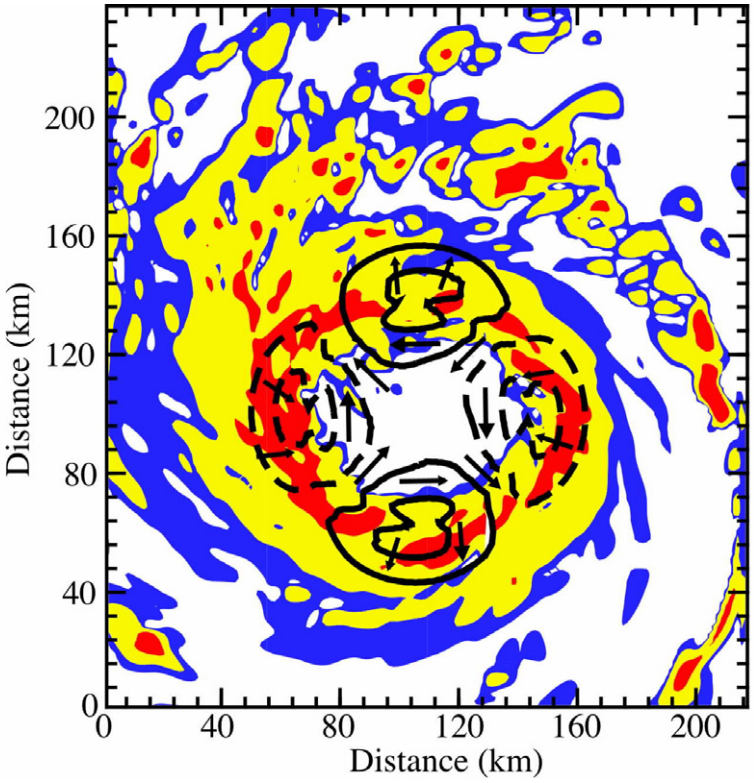

Figure 6-69. Simulated low-level radar reflectivity (shading), with warmer colors indicating heavier precipitation. Contours and vectors indicate pressure and wind perturbations associated with a dynamical instability in the eyewall. Pressure contours are drawn at values of 0.5 and 1.5 mb with positive values indicated by solid lines, negative values by dashed lines.

We identify key aspects of the secondary circulation that play important roles in storm intensification. The inflow into the eyewall is very intense within the shallow boundary layer near the ocean surface, but transitions to strong outward flow just above the boundary layer as the air begins its fairly rapid rise within the eyewall (Figure 6-70). As described below, this outflow appears to play an important role in allowing thunderstorms to occur in the eyewall. While many simplified models of hurricanes envision the eyewall as a ring of gradually rising air, our calculations indicate that most of the upward motion in the hurricane eyewall is associated with a small number of intense but isolated thunderstorm updrafts instead of a broader region of more gentle upward motion, consistent with the concept of hot cloud towers.

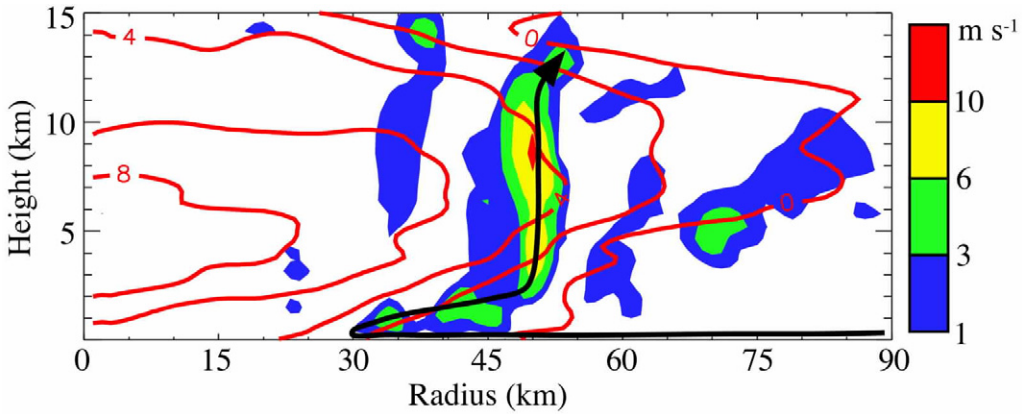

Figure 6-70. Vertical cross section extending outward from the storm center and showing upward vertical motions (shading) and temperature perturbations (red contours, 2 K intervals). The temperatures are perturbations from the model domain average values at each height. The long black arrow shows a hypothetical air parcel trajectory in which the near-surface air penetrates well inside the eyewall so that it resides underneath the warm air in the eye, where convection is suppressed. It then begins to rise slowly and move rapidly outward, eventually moving far enough out from under the warm air that convective instability is released (e.g., near a radius of 50 km).

The eye of the hurricane contains very warm air at upper levels that is generally believed to reduce or prevent the release of thermodynamic instabilities that produce thunderstorms. Some hypotheses suggest that the instability, rather than being released in the vertical direction, is instead released only along a slanted path outward and upward. Figure 6-70 shows that the low-level outward flow in the eyewall displaces the rising air sufficiently far away from the warm air in the eye so that the instability can be released in the vertical direction to produce thunderstorms rather than requiring that the air rise along a slanted path. The energy for these thunderstorms comes from the exchange of heat and moisture from the ocean surface to the low-level inflowing air and is manifested as tongues of warm, moist air within the low-level outward flow that feed into the eyewall thunderstorms.

Scott A. Braun, Code 912 (Scott.A.Braun.1@gsfc.nasa.gov)

Studies of Hurricanes During CAMEX-4

During August and September 2001, NASA sponsored the Convection and Moisture Experiment 4 (CAMEX-4). Camex-4 focused on hurricane research in the eastern Atlantic region. NASA conducted the campaign jointly with NOAA and university scientists. The effort was part of the U.S. Weather Research Program (USWRP) hurricane landfalling program.

The main CAMEX-4 objective was to obtain a comprehensive mapping of the full 3-dimensional structure of hurricanes. The mapping will be used in studies and modeling of processes related to intensification (and weakening) and tracking of hurricanes, especially near landfall. NASA and NOAA scientists designed five experiments to address CAMEX-4 objectives, the USWRP hurricane landfalling objectives, and the NOAA operational tropical storm forecast requirements.

One of the high-priority goals of the Goddard and collaborating UMBC/JCET and GEST scientists was to measure high-altitude temperature and wind simultaneously with radar measurements of the hurricane. As hurricanes mature, heat is produced by condensation as air expands and rises. This process in turn causes a lowering of the hurricane's surface pressure. Lower surface pressures result in air accelerating toward the hurricane center. This movement intensifies the hurricane circulation through the Coriolis force. The heat carried aloft by the rising air produces a characteristic "warm core" in the upper tropopause. In 1998, the CAMEX-3 campaign measured the relation of this warm core to the hurricane's wind and precipitation structure. These measurements were limited to the DC-8's altitude (12 km). Thus, little was known about the temperature and wind structure above that altitude. During CAMEX-4, more emphasis was placed on measuring the full vertical extent of the warm core.

The NASA ER-2 and DC-8 aircraft were instrumented with numerous remote sensing and in situ instruments to provide high-resolution, detailed measurements of the structure of hurricanes. The two NOAA P3 aircraft flew in a coordinated fashion with the NASA aircraft. Two instruments played a key role in measuring the warm core of a mature hurricane. The Goddard ER-2 Doppler Radar (EDOP) is a downward-looking instrument that measures radar reflectivity and vertical velocity in precipitation regions. The ER-2 High-altitude Dropsonde system (EHAD) was a joint effort between JCET's Jeff Halverson and NCAR.

For the first time during CAMEX-4, high-altitude dropsondes were released by EHAD into a hurricane while simultaneous radar measurements were taken by EDOP. Figure 6-71 shows a pass across Hurricane Erin on 10 September 2001 with EDOP. Erin was a mature storm with an unusually clear eye and eyewall. The reflectivity and Doppler measurements provide a clear indication of the outwardly sloping eyewall in the storm. During this pass and others, the ER-2 and DC-8 aircraft launched dropsondes to map Erin's temperature and wind structure. Figure 6-72 provides a temperature and moisture sounding from one of the first high-altitude ER-2 dropsondes, which was launched into a hurricane eye. These data sets are being analyzed to more fully understand the dynamics related to hurricane intensification.

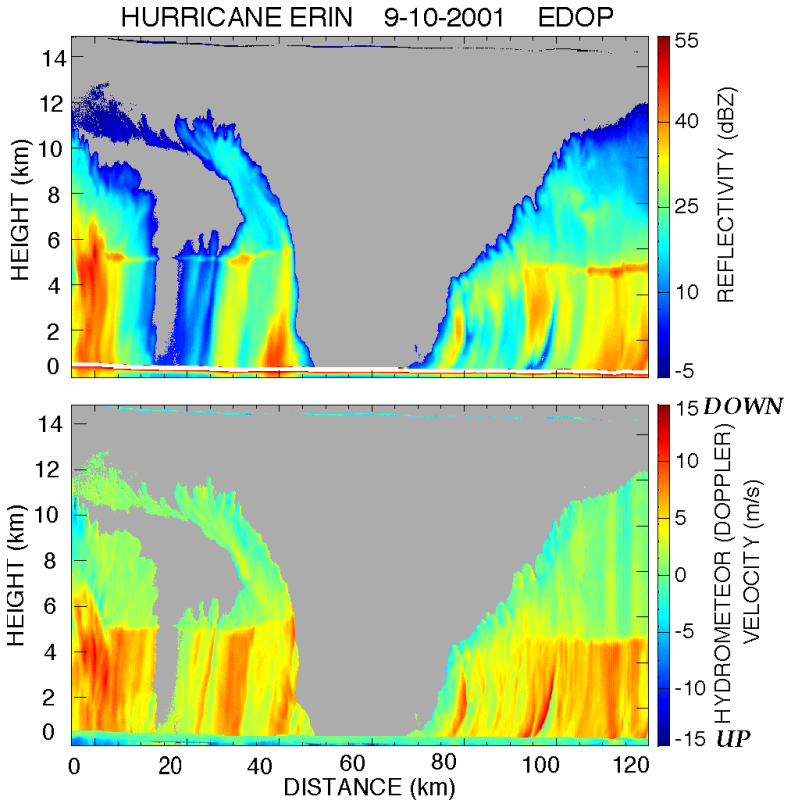

Figure 6-71. EDOP measured vertical structure of Hurricane Erin. The top panel shows the radar reflectivity and the bottom panel shows the Doppler velocity.

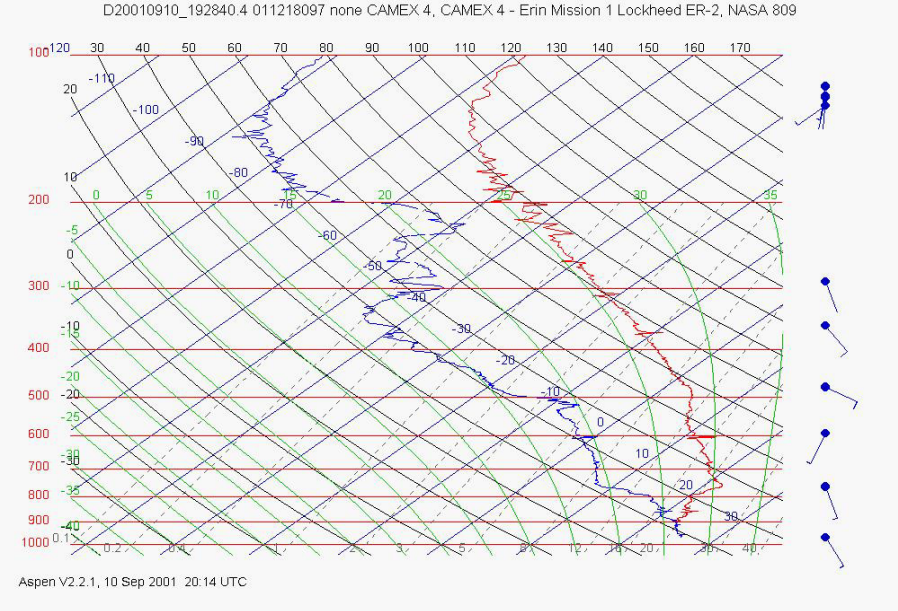

Figure 6-72. First dropsonde released by the ER-2 High Altitude Dropsonde (EHAD) into the ER-2 into the eye of a hurricane during Hurricane Erin .

Gerald Heymsfield, Code 912 (Gerald.M.Heymsfield.1@gsfc.nasa.gov)

Physical Processes

Global Solar Oscillations

A wide variety of oscillation modes can exist inside the Sun. Most cover the entire globe. Modes with short oscillation periods are easiest to detect and have been recorded by the thousands. Beat periods between various modes range from minutes to many years. Long beat periods that affect solar luminosity might affect the Earth's climate.

The family of Rossby modes propagate in the Sun's convection region, which occupies the outer third of its radius. Astronomers call these *r-modes*. The Rossby *waves* of meteorology are local approximations to the Rossby *mode* of a sphere. All are driven by the Coriolis force. Rossby modes rotate more slowly than the fluid in which they oscillate—they drift "backwards." This behavior normally distinguishes them from the other solution to the same equations—a stationary geostrophic flow. But the distinction is weakened by solar differential rotation (i. e., an altitude-dependent zonal wind). Such a wind makes Rossby and geostrophic motion more similar. A geostrophic flow begins to drift backwards too, and, with increasing wind strength, it eventually becomes identical to a Rossby mode[1].

Gravity modes are another type of oscillation that also defines long beat periods of months or years in the Sun. These beats with precisely known periods affect the timing of fluctuations in solar activity (sunspots, flares, and ejections of mass into the planetary system).[2] Thus, danger levels for astronauts and space equipment should become a bit more predictable by taking into account these very stable modes. Whether their long-term modulation of the solar energy output is large enough to affect the Earth's climate is under investigation.

Finally, the prominence of beats means that nonlinear amplitudes are involved, causing gravity modes to deposit considerable energy in layers just below the solar convection zone. This would drive a significant reversing zonal flow, analogous to the QBO (Quasi-Biennial Oscillation) in the Earth's atmosphere, that is conjectured to possibly be a main energy source for the 11-year solar activity cycle. [3]

Charles L. Wolff, Code 915 (Charles.L.Wolff.1@gsfc.nasa.gov

[1] C.L. Wolff, Astrophysical Journal, 502, 961, 1998
[2] C.L. Wolff, Astrophysical Journal, 264, 667, 1983
[3] H.G. Mayr, C.L. Wolff, & R.E. Hartle, Geophysical Research Letters, 28, 463, 2001